Materials Today Bio 31 (2025) 101518

Contents lists available at ScienceDirect

Materials Today Bio

journal homepage: www.journals.elsevier.com/materials-today-bio

Multi-targeted nanogel drug delivery system alleviates neuroinflammation and promotes spinal cord injury repair

Penghui Wang [a,b,1], Zaifeng Chen [a,1], Ping Li [b], Abdullah Al Mamun [c], Shaoxia Ning [b], Jinjing Zhang [a], Chonghui Tang [a], Tianmiao Sun [a,b], Jian Xiao [a,b,c], Xiaojie Wei [a,b,*], Fenzan Wu [a,b,**]

[a] Affiliated Cixi Hospital, Wenzhou Medical University, Ningbo, Zhejiang, 315300, China
[b] Cixi Biomedical Research Institute of Wenzhou Medical University, Ningbo, Zhejiang, 315300, China
[c] Central Laboratory of the Lishui Hospital of Wenzhou Medical University, Lishui People's Hospital, Lishui, Zhejiang, 323000, China

ARTICLE INFO

Keywords:
Spinal cord injury
Neuroinflammation
Quercetin
Target
Drug delivery system

ABSTRACT

Spinal cord injury (SCI) is significantly hampered by an inflammatory microenvironment, prompting continued efforts in drug development to address inflammation. Research shows that quercetin (Que) exhibits excellent performance in reducing inflammation and neuroprotection. However, its application is limited by poor solubility, notable side effects, and the unique pathophysiology of the spinal cord. In this study, we introduce a novel multifunctional liposome hydrogel drug delivery system (QLipTC@HDM), obtained by incorporating liposomes with blood-spinal cord barrier penetration and injury site targeting properties (LipTC) into a dual-network viscous hydrogel (HDM). Our results demonstrate that encapsulating Que in LipTC (QLipTC) enhances solubility, minimizes toxic side effects, facilitates lesion targeting, and aids in crossing the blood-spinal cord barrier. Moreover, encapsulation in HDM significantly prolongs the retention of QLipTC at the injury site after local administration. Crucially, our findings reveal that QLipTC@HDM induces M2 phenotype transformation in glial cells and in mice with SCI, thereby mitigating inflammation. This intervention additionally preserves the integrity of the blood-spinal cord barrier, optimizes the spinal cord microenvironment, reduces glial scarring, promotes axonal regeneration, and enhances motor function recovery in SCI mice. In summary, our investigations highlight the potential of this disease-specific drug delivery system as a promising therapeutic approach for the treatment and management of SCI.

1. Introduction

Spinal cord injury (SCI) causes permanent impairment to sensory, motor and autonomic nerves, resulting in lifelong paralysis [1–3]. Primary SCI results in blood vessels rupture, tissue ischemia, vascular edema. Within minutes, the injured area recruits local microglia, which are activated into multiple phenotypes to regulate neuroinflammation. Moreover, persistent infiltration of inflammatory cells leads to apoptosis, cystic cavities, and neuronal atrophy [4]. Therefore, inflammatory response is a core pathological process in SCI and plays a crucial role in the clinical prognosis [5]. Effectively controlling secondary inflammatory reactions is beneficial for stabilizing the spinal cord's microenvironment, promoting neural axonal growth, and improving injury repair [6,7].

Quercetin (Que), as a flavonoid compound, exhibits significant anti-inflammatory and antioxidant effects in the treatment of central nervous system injury [8]. Through intraperitoneal injection or oral administration, it effectively promotes the polarization of M1-type microglia to M2-type [9–11], regulates the microenvironment [12], protects neurons, and enhances motor function in mice with SCI [13,14]. This suggests significant potential for its application in SCI treatment. However, the therapeutic efficacy of Que in SCI is often limited by its poor solubility, low bioavailability, significant side effects and the unique pathological and physiological environment of the spinal cord [15,16]. Several drug delivery systems have been developed to enhance the solubility of Que and increase its bioavailability, such as phospholipid

* Corresponding author. Affiliated Cixi Hospital, Wenzhou Medical University, Ningbo, Zhejiang, 315300, China.
** Corresponding author. Affiliated Cixi Hospital, Wenzhou Medical University, Ningbo, Zhejiang, 315300, China.
E-mail addresses: weixj5100@126.com (X. Wei), wufenzan@163.com (F. Wu).
[1] These authors contribute equally to this work.

https://doi.org/10.1016/j.mtbio.2025.101518
Received 23 June 2024; Received in revised form 26 December 2024; Accepted 22 January 2025
Available online 23 January 2025

complex [17], self-nanoemulsifying drug delivery system [18], or germanium nanoparticle [19].

Liposome nanoparticles offer unique advantages in enhancing the dissolution of drugs and have been widely used for encapsulating and delivering drugs [20–22]. However, they face several constraints in delivering and targeting drug accumulation effectively within the injury site [20,23]. The blood-spinal cord barrier specifically prevents liposomes from entering spinal cord lesions [24]. It has been shown that surface modifications of nanoparticles can significantly improve drug permeability. A glucose-modified Que liposome was reported to penetrate the blood-brain barrier and deliver more Que to brain tissue to enhance its neuroprotective effect [25]. The blood-spinal cord barrier was crossed with Que-loaded extracellular vesicles to prevent its degradation [26]. Transactivator of transcription (TAT) peptides, which contain positively charged protein transduction domains, facilitate transmembrane crossing by interacting with negatively charged cell membranes [27,28]. Besides, environmental factors (MMPs, CSPGs, ROS, etc) have also become effective targets for targeted drug therapy following SCI. A reactive oxygen species-responsive mitochondria-targeted liposomal was reported to encapsulate the Que to reduce neuroinflammation, oxidative stress, and apoptosis [29]. And CAQK peptide was used to precisely target the injured spinal cord regions by recognizing the CSPGs [30–32]. Including both membrane-penetrating and targeting functionalities in nanoparticles is beneficial for dual-targeted therapeutic effects.

Nano-pharmaceutics are adversely affected by a lack of specific distribution and insufficient drug accumulation during intravenous delivery [24]. An increasing number of studies employ gel-based in situ delivery systems for Que to mitigate their non-specific distribution toxicity and improve therapeutic efficacy. It has been reported that Que-combined collagen-polypyrrole composite could induce cell differentiations, and act as an excellent strategy for spinal cord regeneration [33]. And hydrogel containing nano-pharmaceutics can further enhance its drug-carrying capacity and functionality [34,35]. It has been reported that Que-based alginate nanogels could efficiently bypass the BBB via the nose-to-brain pathway and enhance the antidepressant effects [36]. Additionally, Que-filled nanostructured lipid carriers can be formulated into an intranasal in situ gel to improve brain targeting [37]. Moreover, viscous gel plays an important role in drug retention at the injured site, which can effectively reduce the loss and dispersion of drugs [38,39]. The incorporation of targeted liposomes and adhesive hydrogels is anticipated to enhance drug absorption via diverse targeted mechanisms, thereby augmenting the therapeutic efficacy of Que. However, there is a limited number of studies focusing on the in situ gel delivery of Que in the context of SCI.

Herein, we designed and synthesized a multifunctional Que-loaded liposomal gel drug delivery system (QLipTC@HDM) to achieve the anti-inflammatory and neuroprotective effects following SCI (Fig. 1). Liposomal encapsulation improves the solubility of Que. By utilizing the interaction between TAT peptide and negatively charged cell membranes to facilitate transmembrane penetration [28,40,41] as well as the specific affinity of CAQK peptide towards CSPGs secreted in large quantities at the site of SCI [32], we have simultaneously grafted the TAT peptide and CAQK peptide onto the liposomes (LipTC) to facilitate targeted delivery of the drug across the blood-spinal cord barrier to the injured site. Drug-loaded liposomes (QLipTC) are further incorporated

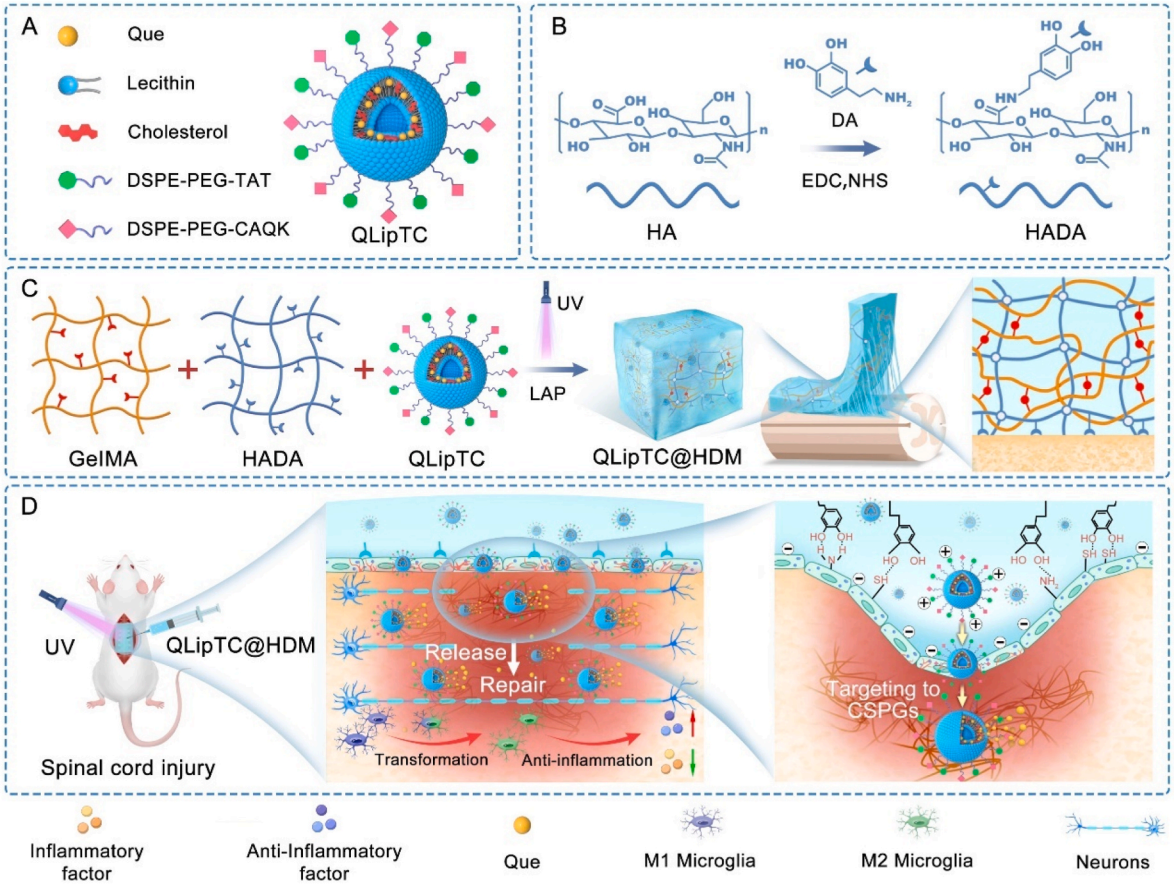

Fig. 1. Schematic illustration of the preparation of the transmembrane-targeted nanogel drug delivery system (QLipTC@HDM) and its application in spinal cord injury repair. (A) Schematic diagram of transmembrane-targeted liposomes (QLipTC). (B) Synthesis route of HADA. (C) Synthesis and dual network schematic of QLipTC@HDM. (D) Application of QLipTC@HDM in spinal cord injury repair, leveraging HDM to prolong drug retention at the injury site and LipTC to facilitate Que penetration across the blood-spinal cord barrier for targeted retention at the injury site, thereby exerting potent anti-inflammatory and neuroprotective effects.

into a dual-network viscous gel (HGM) formed by bonding dopamine and hyaluronic acid-grafted polymers (HADA) together with methacrylate gelatin (GelMA). Que is more efficiently utilized through multi-directional in situ administration at the site of SCI. Our studies have demonstrated that QLipTC@HDM can exert the promising anti-inflammatory effects of Que and promote SCI repair. This study suggests that LipTC@HDM can be an effective drug delivery system for treating SCI and finding applications in biomedical fields.

2. Materials and methods

2.1. Materials

Gelatin methacryloyl (GelMA) was purchased from Suzhou Yongqinquan Intelligent Equipment Co., Ltd. Quercetin (Que), and Evans Blue were purchased from Sigma-Aldrich (MO, USA). Hyaluronic acid (HA) was purchased from Rhawn (Shanghai, China). Dopamine (DA), phospholipids, and cholesterol were purchased from Aladdin (Shanghai, China). DSPE-PEG3.4K, DSPE-PEG3.4K-Mal, and DSPE-PEG-FITC were purchased from Xian Ruixi Biotechnology Co., Ltd. (Shangxi, China). TAT and CAQK were synthesized from Shanghai Qiangyao Biotechnology Co., Ltd. (Shanghai, China). CSPGs (CC117) were purchased from Millipore (MA, USA). Enhanced CCK-8 reagent was purchased from Beyotime Biotechnology (Shanghai, China). DMEM, fetal bovine serum, penicillin-streptomycin solution, and 0.25 % trypsin-EDTA were purchased from Gibco (NY, USA). Mouse TNF-a ELISA Kit, Mouse IL-10 ELISA Kit and Mouse IL-6 ELISA Kit were purchased from Solarbio (Beijing, China).

2.2. Preparation and characterization of DSPE-PEG-TAT and DSPE-PEG-CAQK

DSPE-PEG-TAT and DSPE-PEG-CAQK were synthesized through thiol maleimide reaction by combining TAT or CAQK with DSPE-PEG-Mal and allowing them to react under nitrogen protection for 24 h. The resulting mixture underwent dialysis (MWCO: 3500) to eliminate unreacted components, followed by freezing. The lyophilized products were then dissolved in deuterated DMSO to acquire ^{1}H NMR spectra utilizing an Oxford NMR AS400 spectrometer. The infrared spectrum was obtained using a Fourier infrared spectrometer.

2.3. Synthesis and characterization of Que-loaded transmembrane-targeted liposomes (QLipTC)

The preparation of QLipTC involves the solvent evaporation method. A mixture of soy lecithin, cholesterol, DSPE-PEG, DSPE-PEG-TAT, DSPE-PEG-CAQK (in a molar mass ratio of 60: 20: 8: 4: 4) and Que was dissolved in anhydrous ethanol. This mixture was then slowly injected into PBS at 50 °C under vigorous stirring to facilitate ethanol evaporation. A cell disruptor (JY92-IIN, Scientz) was used for ultrasonic treatment (300 W, 3 s on/5 s off) for 5 min, followed by extrusion through a 0.22 μm membrane to produce QLipTC. To prepare the fluorescent liposomes (FITC-LipTC), DSPE-PEG-FITC was used instead of DSPE-PEG. The loading and encapsulation efficiency of Que were determined using a multifunctional microplate reader after high-speed centrifugation (12000 rpm, 20 min) of the supernatant. The encapsulation rate was calculated as (Total Que content - Free Que content)/Total Que content, and the drug loading amount was calculated as (Total Que content - Free Que content)/liposomes content. The particle size and zeta potential of the liposomes were assessed utilizing a laser nanoparticle size analyzer, and the stability of the liposomes was evaluated by monitoring the particle size and zeta potential during storage. Morphological analysis was conducted using a transmission electron microscope (JEM 1200EX, JEOL). Liposomes were deposited on a 200-mesh copper grid, stained with 2 % phosphotungstic acid for 10 min, and examined under a transmission electron microscope.

2.4. Synthesis and characterization of HDM and QLipTC@HDM

The dual-network hydrogel (HDM) is synthesized by combining GelMA and HADA, followed by crosslinking under 405 nm light irradiation. The HADA polymer is synthesized by grafting hyaluronic acid (HA) with dopamine (DA). Specifically, the components—hyaluronic acid (HA) (3 mmol), EDC (1 mmol), NHS (1 mmol), and dopamine hydrochloride (3 mmol)—are dissolved in MES buffer and allowed to react under a nitrogen atmosphere for 48 h. The resultant mixture is subjected to dialysis using a dialysis bag with a molecular weight cut-off (MWCO) of 10,000 to isolate HADA. The synthesized HADA is subsequently characterized through nuclear magnetic resonance (NMR) and ultraviolet (UV) spectroscopy. A HDM pre-gel solution is formulated by combining 20 % HADA with 20 % GelMA in a 1: 2 vol ratio. QLipTC@HDM is then prepared by integrating QLipTC into the HDM pre-gel solution, followed by photoinitiated crosslinking. The microstructure of HDM was investigated using scanning electron microscopy (Hitachi S-3000N), and its adhesion strength was subsequently analyzed.

2.5. Barrier penetration and targeting properties detection

The in vitro blood-spinal cord barrier (BSCB) model was constructed using the Transwell system to evaluate the barrier penetration and chondroitin sulfate proteoglycans (CSPGs) targeting ability of LipTC. Briefly, human umbilical vein endothelial cells (HUVECs) were seeded at a density of 1×10^5 cells per well in the upper chamber of the Transwell and cultured for 3 days to establish a tight monolayer. The lower chamber of the Transwells was treated with CSPGs to assess the barrier penetration and CSPGs targeting ability of FITC-LipTC by measuring the fluorescence intensity that passed from the upper chamber to the lower chamber. Additionally, SHSY5Y cells were used to replace CSPGs in the lower chamber of the Transwells, and the ability of the FITC-LipTC to traverse the bilayer cell membrane was evaluated by measuring the fluorescence intensity in the SHSY5Y cells using a laser confocal microscope (STELLARIS 5, Leica). Fluorescence quantification analysis was performed using Image J software. The retention performance of the drug delivery system at the site of SCI in mice was evaluated using a small animal imaging system. ICG@GelMA, ICG@HDM, ICG-Lip@HDM, and ICG-LipTC@HDM were administered at the SCI site, and in vivo fluorescence imaging was performed at 6, 12, 24, 48, and 72 h post-administration using the IVIS Lumina XRMS Series III system (PerkinElmer). At 72 h, the spinal cords were harvested for ex vivo imaging. The retention performance of the drug delivery systems at the injury site was analyzed by evaluating the fluorescence intensity.

2.6. Drug release experiment

To evaluate the drug release profile, a fluorescent substance (DiI) was utilized as a substitute for Que. Briefly, 2 μg of DiI was encapsulated into LipTC, LipTC@GelMA, and LipTC@HDM to create DiI-LipTC, DiI-LipTC@GelMA, and DiI-LipTC@HDM formulations. These samples were placed in a plate containing 3 mL of PBS at 37 °C. Each sampling point involved withdrawing 300 μL of the release medium, and fresh PBS was replenished after each collection time point at 1 h, 2 h, 4 h, 8 h, 12 h, 1 d, 2 d, 3 d, 5 d, 7 d, 9 d, 10 d, 12 d, 14 d, 16 d, 18 d, and 21 d. The fluorescence intensity of DiI was measured using a fluorescence microplate reader, and the cumulative release was calculated.

2.7. In vivo degradation experiment

The in vivo degradation behavior of the hydrogel was evaluated by monitoring the alterations in the weight of the gel at various time intervals following subcutaneous implantation. Sterile HDM and GelMA hydrogels were implanted into the dorsal subcutaneous tissue of mice. The gel samples were retrieved at 1, 3, 7, 14, and 21 d post-implantation,

and the residual weight was measured to determine the extent of degradation.

2.8. Cell viability assay

The impact of the drug delivery system on cell viability was assessed using the CCK-8 cell viability assay kit. Cell suspensions (1×10^5 cells/100 μL) were seeded in 96-well plates and co-cultured with the drug for 24, 48, and 72 h. Subsequently, the cell culture medium was replaced with 10 % CCK-8 solution, and the absorbance at 450 nm was measured after a 2 h incubation. Additionally, Calcein AM/PI staining assay was employed to evaluate the effects of the drug delivery system on the viability and morphology of PC12 and BV2 cells. Cells were cultured in 12-well plates and treated with the drug for 24, 48, and 72 h. Following incubation, cells were stained with Calcein AM/PI, and images were acquired using a DMILLED inverted fluorescence microscope (Leica).

2.9. Flow cytometer

The polarization levels of BV2 cells were analyzed by flow cytometry. In brief, BV2 cells were treated with various drugs for 24 h, followed by collection and washing with a cold buffer solution. They were then incubated with antibodies against CD206 (BD, 565250), CD86 (BD, 742120), and CD11b (BD, 557396), and the expression of CD206 and CD86 was analyzed using a flow cytometer. Further analysis was conducted using FloJo software.

2.10. SCI model and treatment

A total of 150 female C57BL6 mice weighing between 18 and 20 g were procured from Vital River Laboratory Animal Technology Co., Ltd. and housed at the Institute of Biomedical and Pharmaceutical Sciences of Wenzhou Medical University. The experimental protocols and animal handling procedures were conducted in accordance with the guidelines of the Experimental Animal Ethics Committee at Wenzhou Medical University (Approval Number: wydw2020-0313). The mice were randomly divided into five groups: Sham (underwent laminectomy without SCI), SCI, SCI + HDM, SCI + QLipTC, and SCI + QLipTC@HDM. Prior to surgery, the mice were fasted overnight and subsequently anesthetized with 1 % pentobarbital sodium (125 μL/20g). SCI was induced by impacting the spinal cord using a precise spinal cord impactor (YHCI99, Wuhan Yihong Technology Co., Ltd.) at a depth of 0.8 mm, with an impact velocity of 3.5 m/s, and a dwell time of 50 ms. Following SCI, the mice in the SCI group were administered 0.9 % NaCl as a control. The QLipTC@HDM group received a treatment consisting of 30 μL of a QLipTC@HDM pre-gel solution, which was thoroughly mixed and dropped onto the SCI surface. This was immediately followed by exposure to 405 nm light for 30 s to promote in situ gelation. In contrast, the HDM group received a treatment without QLipTC encapsulation, using the same administration method as the QLipTC@HDM group. The QLipTC group was administered the treatment via a tail vein injection of 100 μL of the solution, without incorporation into the gel. Unless otherwise specified, the dosage of Que in both the QLipTC and QLipTC@HDM groups was at 500 μg/kg. Following administration, the muscles and skin were sutured and maintained at 37 °C until recovery. Penicillin was administered through intramuscular injection for the initial three days post-injury. Manual bladder emptying was conducted daily until the restoration of autonomous micturition function.

2.11. Functional behavioral assessment

Motor function post-SCI was evaluated using the Basso Mouse Scale (BMS) scoring system. Hind limb motor function scores were assessed by two blinded observers at 1, 3, 7, 14, 21, and 28 days post-SCI. On day 28, hind limb gait was analyzed using the footprint analysis method. Mice were placed on a narrow track (0.02 m wide x 0.5 m long) with their forelimbs marked in blue ink and hind limbs marked in red ink. The hind limb movements were recorded on day 28. Subsequently, neuroelectrophysiological detection was employed to assess motor evoked potentials (MEPs). Mice were anesthetized before the examination, and the implantation of electrodes was conducted following the previous study [42]. The recovery of mobility was reflected by stimulating the spinal cord and recording MEP values. Further assessment of the muscle and urination function by analyzing the size and weight of the hind limb gastrocnemius muscle and the bladder.

2.12. Western blot assay

The BCA protein assay kit (BioVision, P0010) was utilized to determine protein concentrations in cells or spinal cord tissues. Proteins were separated by SDS-polyacrylamide gel electrophoresis (SDS-PAGE) and subsequently transferred onto PVDF membranes. The membranes were then probed with specific antibodies, including TNF-α antibody (Proteintech, 26405-1-AP), IL-6 antibody (Proteintech, 00097020), Arginase antibody (ZEN BIO, KK0819), CD86 antibody (Abcam, ab239075), β-actin antibody (ZEN BIO, KK1231), MBP antibody (Abcam, ab7349), Tuj-1 antibody (Abcam, ab18207), Bax antibody (Proteintech, 50599-2-Ig), Bcl-2 antibody (Proteintech, 00113524), GFAP antibody (Affinity, DF6040), and NF200 antibody (Abcam, ab4680), followed by incubation with corresponding secondary antibodies. The protein bands were visualized using the ChemiDicTM XRS + Imaging System, and their intensities were quantitatively analyzed using Image J software.

2.13. Immunofluorescence staining

The spinal cord tissue was embedded in paraffin and sectioned into 5 mm thick slices. HE and Nissl staining reagents were employed to stain the tissue sections, which were then examined using an optical microscope (Nikon, Japan). The cells and tissue sections underwent pretreatment with a 5 % BSA solution for 1 h, followed by incubation with CD86 antibody (1:500, Abcam, ad239075, for labeling M1 type microglia), Arginase antibody (1:100, Proteintech, 16001-1-AP, for labeling M2 type microglia), mouse anti-GFAP antibody (1:200, CST, #3670, for labeling astrocyte), rabbit anti-Tuj-1 antibody (1:200, Abcam, ab18207, for labeling immature and mature neurons), chicken anti-NF200 (1:5000, Abcam, ab4680, for labeling axonal neurons), and rabbit anti-MBP (1:200, Abcam, ab40390, for labeling myelin basic protein) at 4 °C overnight. Subsequently, the sections were incubated for 1 h at 37 °C with Alexa 488, 594, or 647-conjugated secondary antibodies (1:1000, Abcam). Finally, the sections were mounted in a DAPI-containing mounting medium (Solarbio, Beijing, China) and imaged using a confocal laser microscope. To avoid autofluorescence in tissue sections, TrueVIEW autofluorescence quenching kit (Vector Laboratories, Burlingame, California, USA) was used.

2.14. Statistical analysis

Quantitative experimental results were presented as mean ± standard deviation (SD). Statistical significance was assessed using one-way analysis of variance, followed by Tukey's multiple comparison test. Group comparisons were performed using GraphPad Prism software, with statistical significance defined as a p-value less than 0.05. The experiments were replicated three times with representative results.

3. Results

3.1. Preparation and characterization of transmembrane targeted liposomes (QLipTC)

The blood-spinal cord barrier impeded the entry of conventional liposomes, typically used as drug carriers, into the lesion. This study synthesized transmembrane-targeted liposomes (QLipTC) employing a

solvent evaporation method, aimed at enhancing drug delivery to spinal cord lesions. The lipids DSPE-PEG-TAT and DSPE-PEG-CAQK were synthesized using the thiol maleimide coupling method to confer transmembrane and targeting capabilities. The absence of the maleimide peak at 6.77 ppm in the ^{1}H NMR spectrum (Fig. 2A) and the persistence of characteristic DSPE and PEG peaks at 1.25 ppm, 0.88 ppm, and 3.65 ppm indicated successful coupling. Further, FTIR spectroscopy confirmed the synthesis, showing removal of the maleimide peak at 1707 cmˆ-1 and presence of the amide peak at 1664 cmˆ-1 (Fig. 2B). These lipids were combined with cholesterol, phospholipids, and the drug Que to formulate Que-loaded transmembrane-targeted QLipTC. These liposomes exhibited a spherical morphology with an average particle size of 160.142 ± 3.25 nm and a polydispersity index (PDI) of 0.194 ± 0.512 (Fig. 2C). Notably, QLipTC demonstrated a positive zeta potential of 29.44 ± 2.03 mV compared to QLip (−10.37 ± 2.03 mV), enhancing compatibility with negatively charged cell membranes and promoting cellular uptake (Fig. 2D). Stability tests over 21 days showed minimal changes in particle size and zeta potential (Fig. 2E–S1A-I). The encapsulation efficiency for Que was high at 91.63 ± 1.51 % (Fig. 2F). Toxicity assays using BV2 and PC12 cells indicated that Que concentrations exceeding 200 μmol/L were cytotoxic and poorly dispersed in the culture medium (Fig. 2G, Figs. S1J and K). However, QLipTC encapsulation at 200 μmol/L Que improved drug solubility and reduced cytotoxicity, enhancing cell survival (Fig. 2G, Figs. S1J and K).

In an in vitro blood-spinal cord barrier model, CSPGs were used to test QLipTC's barrier penetration and targeting efficacy (Fig. S2). Fluorescence measurements showed that the FITC-LipTC group

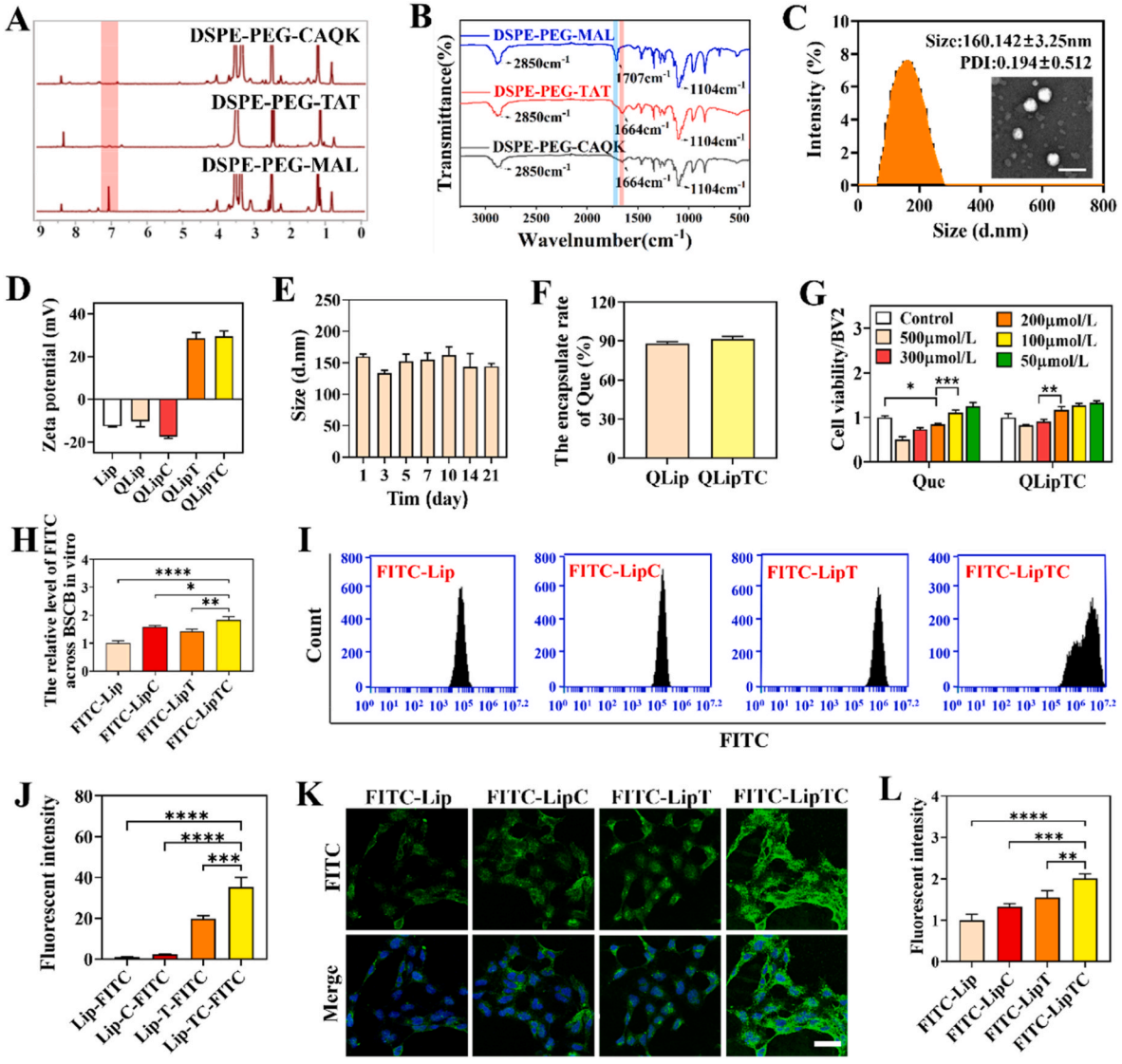

Fig. 2. Preparation and characterization of QlipTC. (A) ^{1}H NMR spectra of DSPE-PEG-CAQK, DSPE-PEG-TAT, and DSPE-PEG-MAL. (B) FTIR spectra of the molecular composition of DSPE-PEG-CAQK, DSPE-PEG-TAT, and DSPE-PEG-MAL. (C) Transmission electron microscopy image of QLipTC along with hydrodynamic radius and polydispersity index assessment. (D) Statistical analysis of ζ potentials of Lip, QLip, QLipC, QLipT, and QLipTC. (E) The particle size variation of QLipTC over 21 consecutive days. (F) Encapsulation efficiency of Que in QLip and QLipTC. (G) CCK-8 assays were performed to evaluate the viability of BV2 cells treated with different concentrations of Que and QLipTC for 24 h. (H) Fluorescence intensity analysis of FITC-labeled formulations (FITC-Lip, FITC-LipC, FITC-LipT, and FITC-LipTC) traversed from the upper chamber to the lower chamber of Transwell. (I) Flow cytometry analysis of the fluorescence intensity of FITC-labeled formulations traversed from the upper chamber and entered the cells located in the lower chamber of the Transwell. (J) Quantitative analysis of the fluorescence intensity obtained from flow cytometry analysis. (K) Representative fluorescence images of FITC-labeled formulations traversed the upper chamber and entered the cells located in the lower chamber of the Transwell. Scale bar is 50 μm. (L) Quantitative analysis of fluorescence intensity in (K). *for $p < 0.05$, ** for $p < 0.01$, *** for $p < 0.001$, **** for $p < 0.0001$.

exhibited the strongest intensity, indicating superior drug transport across the barrier (Fig. 2H). Fluorescence uptake detection of BV-2 and SHSY5Y cells using flow cytometry and confocal microscopy showed that the FITC-LipTC group had stronger cellular fluorescence accumulation compared to other liposomal formulations (Fig. 2I–L).

3.2. Preparation and characterization of LipTC@HDM

Encapsulating liposomes in a viscous gel can enhance their retention at the injury site, thereby promoting sustained therapeutic effects. In this study, HADA viscous polymer and GelMA were cross-linked to form a dual-network viscous gel (HDM) (Fig. S3A). The ^{1}H NMR spectroscopy revealed a hydrogen absorption peak on the benzene ring of DA between 6.8 and 7.2 ppm, confirming the formation of HADA (Fig. 3A). The characteristic UV–visible absorption peak of catechol at 280 nm further confirmed the successful synthesis of HADA (Fig. 3B). The HDM hydrogel is synthesized by mixing 20 % HADA and 20 % GelMA in a 1:2 vol ratio, followed by exposure to 405 nm light irradiation.

Scanning electron microscopy (SEM) revealed that HDM exhibited a reduced pore size relative to GelMA alone, as shown in Fig. 3C, a characteristic essential for ensuring controlled drug release. To evaluate the effect of LipTC@HDM on drug release, DiI was utilized as a substitute for Que in the liposomal formulation. The release studies showed a sustained release over extended periods: LipTC exhibited a release duration of 7 days (91 % ± 1.74), LipTC@GelMA sustained release for 12 days (85.63 % ± 2.44), and LipTC@HDM extended release for 16 days (82.57 % ± 5.33). These findings underscore the superior capacity of HDM for prolonged drug delivery, as illustrated in Fig. 3D. The degradation profile indicates that both GelMA and HDM hydrogels undergo a gradual decline for approximately 21 days after subcutaneous implantation (Fig. 3E). Rheological tests showed that HDM formed a stable gel within a 0.1–10 rad/s frequency range (Fig. S3B). Adhesion performance analysis indicates that HDM exhibits strong adhesion properties to biological tissues, demonstrating effective adherence to organs, the spinal cord, and glass substrates (Fig. 3F–S3C). Fluorescence imaging analysis showed that the ICG-LipTC@HDM group exhibited sustained and robust fluorescence at the injury site for up to 72 h, markedly surpassing the performance of the ICG-GelMA group, which showed negligible detectable fluorescence. During ex vivo imaging of spinal cord tissue, the injured regions in the ICG-LipTC@HDM group exhibited the highest fluorescence intensity. This result may be attributed to the low adhesive properties and larger pore structures of GelMA. The ICG encapsulated within the GelMA exhibited migration away from the implantation site and diffusion out of the gel, resulting in a rapid fade of fluorescence intensity in the ICG-GelMA group.

Biocompatibility assessments showed that neither GelMA, HADA, HDM, nor QLipTC@HDM significantly altered the activity or morphology of PC12 and BV2 cells detected by CCK8 and live dead cell staining (Fig. 3J–L and S3D-J). Further evaluation of the potential toxicity in major organs, including the heart, liver, spleen, lungs, and kidneys, indicates that the QLipTC@HDM system exhibits favorable biocompatibility and safety in vivo (Fig. S4). These results suggest that QLipTC@HDM exhibits effective sustained drug release capabilities, improved retention performance, and high biocompatibility, thereby establishing it as an excellent delivery system for Que.

3.3. QLipTC@HDM promotes the polarization of microglial cells to the M2 phenotype and suppresses inflammatory responses

The M2 subtype of activated macrophages is known to exert beneficial effects in dampening inflammatory reactions. Initially, the optimal concentration of Que for therapeutic application in vitro was determined by evaluating cellular activity and inflammatory responses following Que treatment. Our research findings demonstrate that QLipTC exerts the most pronounced effect on enhancing cell survival under oxygen-glucose deprivation/reoxygenation (OGD/R) conditions at a loading concentration of 30 μmol/L (Figs. S5A and B). Notably, the optimal efficacy of QLipTC@HDM was observed at a Que loading concentration of 50 μmol/mL, potentially due to the sustained release properties of QLipTC encapsulated within HDM. A subsequent assessment of the anti-inflammatory properties of QLipTC@HDM was conducted utilizing an enzyme-linked immunosorbent assay (ELISA) kit. This evaluation revealed a significant decrease in IL-6 expression and an increase in IL-10 expression at a concentration of 50 μmol/L (Figs. S5C–F). As a result, the 50 μmol/L concentration was selected for further cellular studies. Western blot analysis and ELISA assays were employed to investigate the impact of QLipTC@HDM on the polarization of microglial cells. The results revealed that QLipTC@HDM markedly decreased the levels of M1 pro-inflammatory markers (CD86, IL-6, and TNF-α) induced by OGD/R stimulation, while concurrently enhancing the expression of M2 anti-inflammatory markers (IL-10 and Arginase) (Fig. 4A–H). Immunofluorescence analysis (Fig. 4I–K) and flow cytometry data (Fig. 4L–N) further confirmed that QLipTC@HDM promotes the polarization of microglia towards the M2 phenotype while inhibiting the M1 phenotype. This is evidenced by a decrease in CD86 fluorescence intensity and an increase in CD206 fluorescence intensity compared to the HDM and QLipTC groups. These results suggest that QLipTC@HDM possesses the ability to inhibit neuroinflammation through the regulation of microglial polarization.

3.4. QLipTC@HDM facilitates the polarization of microglial cells towards the M2 phenotype and alleviates the inflammatory response in mice following spinal cord injury

To determine the optimal efficacy of QLipTC@HDM on the inflammatory response post-SCI, various dosages (250 μg/kg, 500 μg/kg, and 1 mg/kg) of Que were evaluated. Five days post-SCI, the levels of inflammatory factors at the lesion site were assessed. The results indicated that at a Que-loaded dosage of 500 μg/kg, the expression levels of IL-6 and TNF-α decreased, while the expression level of IL-10 increased (Figs. S6A–C). Subsequently, a dose of 500 μg/kg of QLipTC@HDM was employed in animal experiments. The QLipTC@HDM treatment group exhibited a significant reduction in IL-6, TNF-α, and CD86 levels, and a significant increase in IL-10 and Arginase levels compared to the QLipTC group alone ($p < 0.01$) (Fig. 5A–H). Furthermore, compared to the SCI group, the immunofluorescence intensity of the M1 microglia marker (CD86) was notably diminished, while the intensity of the M2 microglia marker (Arg1) was significantly elevated in QLipTC@HDM group in the lesion core (Fig. 5I–M). In summary, these findings indicate that QLipTC@HDM administration promotes the transformation of microglial cells into the M2 phenotype and alleviates the inflammatory response in mice following SCI.

3.5. QLipTC@HDM improves the microenvironment of spinal cord lesions, attenuates neuronal death and suppresses glial scar formation in mice following spinal cord injury

The acute phase inflammatory response contributes to enhanced blood-spinal cord barrier (BSCB) permeability, thereby disrupting the spinal cord environment and leading to neuronal death. Evaluation of changes in BSCB permeability revealed that the SCI group exhibited the highest Evans blue content at the spinal cord lesion site 1 h (Fig. 6A–C) or 24 h (Fig. S7) following the tail vein injection of Evans blue dye, which was reduced in QLipTC@HDM intervention group. Notably, QLipTC@HDM treatment led to a significant decrease in the levels of the pro-apoptotic protein Bax and an increase in the expression of the anti-apoptotic protein Bcl-2 (Fig. 6D–F). Moreover, the expression of MBP, Tuj-1, and NF200 was markedly elevated, while GFAP expression was reduced in QLipTC@HDM group (Fig. 6D–G-J). Immunofluorescence analysis revealed weaker fluorescence of NF200 and MBP in the SCI and HDM groups, with enhanced fluorescence observed in the QLipTC group and the strongest fluorescence in the QLipTC@HDM group (Fig. 7A–C).

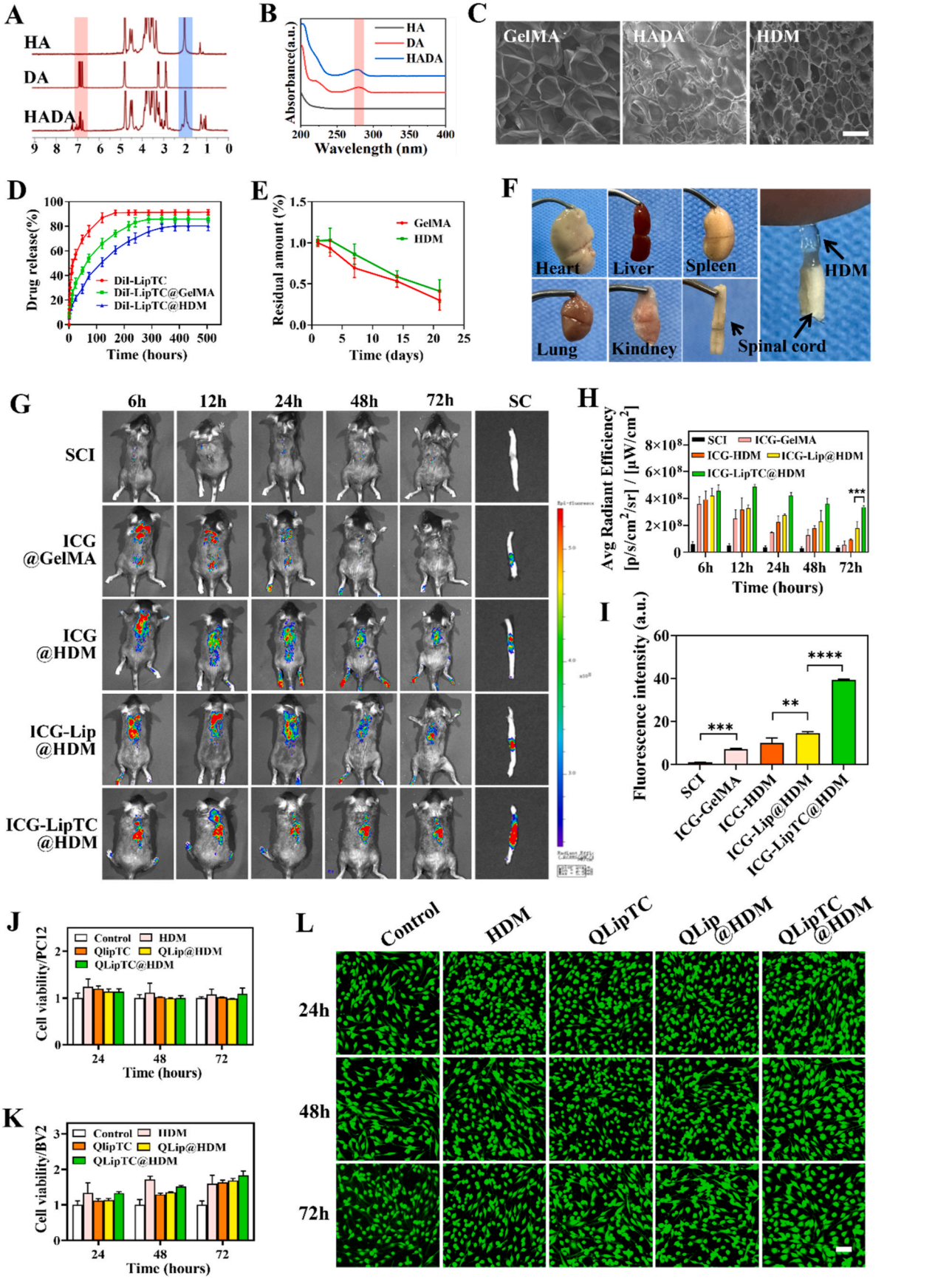

(caption on next page)

Fig. 3. Preparation and characterization of QlipTC@HDM. (A) ^{1}H NMR spectra of DA, HA and HADA. (B) UV absorption spectra of DA, HA, and HADA. (C) SEM images of GelMA, HADA, and HDM. Scale bar is 100 μm. (D) Release profiles of DiI from formulations including LipTC, LipTC@GelMA, and LipTC@HDM. (E) The degradation profile of the GelMA and HDM hydrogel in vivo. (F) Evaluation of the biological tissue adhesion performance of HDM. (G) In vivo fluorescence tracking in mice with SCI using a small animal imaging system at 6, 12, 24, 48, and 72 h post in situ gel application, including fluorescence imaging of isolated spinal cord at 72 h. (H) Quantitative analysis of fluorescence intensities at the injury site in (G). (I) Quantitative analysis of fluorescence intensities in ex vivo spinal cord tissues in (G). (J, K) CCK-8 assays were performed to evaluate the viability of PC12 and BV2 cells treated with different systems for 24, 48, and 72 h. (L) Calcein-AM/PI double staining was performed to detect the survival of PC12 cells treated with different materials for 24, 48, and 72 h, scale bar at 50 μm ** for $p < 0.01$, *** for $p < 0.001$, **** for $p < 0.0001$.

To evaluate nerve growth and glial scar formation, co-staining of GFAP and Tuj-1 was conducted (Fig. 7D–F). The results demonstrated higher fluorescence intensity of GFAP in the SCI and HDM groups, accompanied by reduced Tuj-1 fluorescence. However, treatment with QLipTC@HDM resulted in a reduction of GFAP fluorescence levels and an increase in Tuj-1 fluorescence intensity. Quantitative analysis of the spinal cord lesion volume, based on GFAP fluorescence (Fig. S8), demonstrated a significant decrease in cavity size, with an increase in neural axon infiltration into the lesion center following QLipTC@HDM treatment. These findings suggest that QLipTC@HDM intervention enhances blood-spinal cord barrier permeability, mitigates neuronal death, suppresses glial scar formation, and promotes axonal neuronal growth in mice post-SCI.

3.6. QLipTC@HDM enhances motor function recovery in mice following SCI

The assessment of spinal cord tissue morphology and motor function levels was conducted 28 days post-injury. In Fig. 8A, the severity of hind limb paralysis, as evaluated by BMS motor function scores, was higher in the QLipTC@HDM group compared to the SCI group. Notably, QLipTC@HDM treatment significantly ameliorated hind limb joint flexibility, strength, and coordination, as evidenced by hind limb footprints and joint mobility assessments (Fig. 8B and C). Neurophysiological tests and muscle analyses were conducted to evaluate the motor evoked potentials (MEPs) and muscle function. The findings indicated that the QLipTC@HDM treatment was able to effectively alleviate muscle atrophy and show a noticeable recovery in MEPs in contrast to the SCI group, which exhibited reduced muscle weight and diminished MEP amplitude (Fig. 8D–F). HE and Nissl staining were performed to analyze tissue morphology and neural Nissl function in the injured tissues. The findings revealed a substantial cavity formation at the injury site in mice from the SCI group, accompanied by a significant reduction and atrophy of Nissl bodies (Fig. 8G and H). In contrast, the QLipTC@HDM treatment group exhibited the smallest cavity size and the highest Nissl body count. Bladder function post-SCI was also evaluated to assess recovery from urinary incontinence in mice (Fig. 8I and J). The results indicated that bladder volume and weight were highest in the SCI group, slightly reduced after QLipTC treatment, and lowest in the QLipTC@HDM group. This suggests a partial restoration of autonomous urination function following QLipTC@HDM treatment. These findings indicate that QLipTC@HDM enhances motor function recovery in mice post-SCI.

4. Discussion

Spinal cord injury (SCI) initiates a cascade of inflammatory responses that significantly impede neural regeneration and repair processes. Quercetin (Que), a dietary flavonoid known for its anti-inflammatory properties, has been extensively documented to substantially influence neuroinflammation and neural repair [43,44]. Nonetheless, the utilization of Que within the field of neuroscience is considerably constrained by its poor solubility and low bioavailability. Therefore, the development of an optimal biocompatible scaffold for encapsulation and sustained drug delivery is anticipated to be an efficacious strategy to address this challenge. This study presents an innovative drug delivery system, QLipTC@HDM, designed to efficiently and precisely deliver Que to the SCI site, thereby addressing inflammation-related microenvironmental and neural regeneration issues. Our findings offer a comprehensive elucidation of the system's therapeutic efficacy and its potential application in the treatment of SCI.

Improving the solubility of Que is essential because its poor solubility severely affects its bioactivity and limits its clinical applications. Consequently, various methods and strategies have been developed to overcome the water insolubility of Que, including structural modifications, the use of cyclodextrin complexes, emulsions, and nanoparticles [45,46]. In this study, Que was encapsulated within a lipid bilayer, achieving an encapsulation efficiency of 91.63 ± 1.51 %, and observed a significant improvement in solubility. Furthermore, our findings indicate that Que markedly suppresses cellular activity at concentrations exceeding 200 μmol/L, a prevalent challenge associated with its direct application. The encapsulation and controlled release of Que via QLipTC@HDM mitigates these toxic side effects, thereby enhancing therapeutic efficacy and safety.

The capacity of pharmacological agents to traverse the distinctive BSCB and remain localized at the site of SCI over an extended duration is essential for achieving therapeutic efficacy. This barrier presents a formidable obstacle to the effective delivery of drugs to the injury site. Recent studies have investigated the encapsulation of Que within poly (Ɛ-caprolactone) (PCL) nanoparticles, demonstrating that these Que-loaded nanoparticles exhibit enhanced permeability across the blood-brain barrier (BBB) compared to unencapsulated Que [47]. Studies have employed glucose-modified liposomes to encapsulate Que in neurodegenerative diseases. These glucose-modified liposomes facilitate enhanced penetration of the BBB via glucose transporter 1, thereby exerting antioxidant neuroprotective effects [25]. Most studies on the repair of SCI by Que are primarily conducted through oral administration or intraperitoneal injection. A study used stem cell-derived extracellular vesicles as carriers for Que, which was administered through tail vein injection to target SCI sites [26]. The findings demonstrated that this approach effectively inhibited the activation of microglia towards the M1 phenotype and astrocytes towards the A1 phenotype, thereby facilitating the recovery of motor function in rats with SCI [26]. This study employs TAT peptide-modified liposomes to enhance the translocation of Que across the BSCB. Concurrently, the CAQK peptide is utilized to selectively identify the aberrantly elevated environmental factors at the SCI site, thereby achieving dual functionalities of membrane penetration and targeted delivery. This approach substantially augments the concentration and retention of the therapeutic agent at the injury locus, a finding corroborated by our previous studies [24]. It is conducive to providing a promising strategy for addressing the unique pathophysiological challenges associated with SCI.

Systemic administration is inherently challenged by the problem of nonspecific drug distribution. Moreover, compared to systemic administration, local administration can substantially reduce the required dosage, enhance bioavailability, and minimize systemic adverse effects. To the best of our knowledge, there are no existing reports on the application of in situ delivery of Que for SCI treatment. This study encapsulated QLipTC in a dual-network viscous hydrogel (HDM), with a Que concentration of 500 μg/kg, which was found to achieve sustained therapeutic effects. Furthermore, compared to the conventional GelMA hydrogel, HDM significantly improves adhesive properties, thereby markedly extending the retention time at the injury site following local administration, as evidenced by small animal live imaging. In contrast,

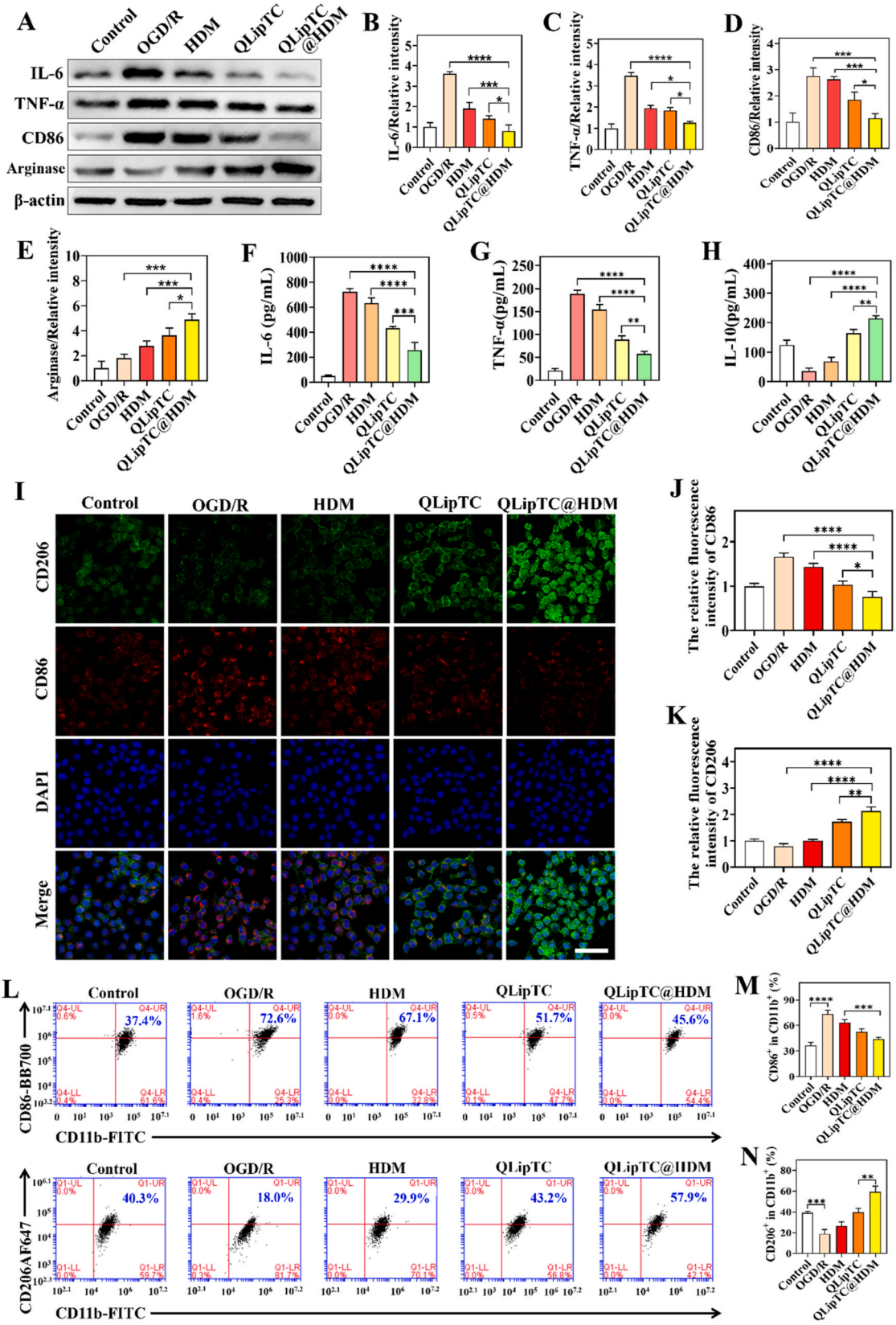

Fig. 4. QLipTC@HDM promotes the transformation of microglia to the M2 phenotype and inhibits the inflammatory response. (A) Western blot analysis of IL-6, TNF-α, CD86, and Arginase protein expressions in each group. (B–E) Quantitative assay of IL-6, TNF-α, CD86, and Arginase protein levels. (F–H) ELISA analysis of the concentrations of IL-6, TNF-α, and IL-10 in BV-2 cells. (I) Immunofluorescence images of CD206 (green), CD86 (red), and DAPI (blue) in BV2 cells following 24 h treatments. The scale bar is 50 μm. (J, K) Quantitative analysis of the mean fluorescence intensity of CD86 and CD206 in each group. (L) Fow cytometric analysis of CD11b/CD86-positive cells and CD11b/CD206-positive cells. (M, N) Quantification analysis of the ratio of $CD86^+$ cells in the $CD11b^+$ population and $CD206^+$ cells in the $CD11b^+$ population. *for $p < 0.05$, ** for $p < 0.01$, *** for $p < 0.001$, **** for $p < 0.0001$.

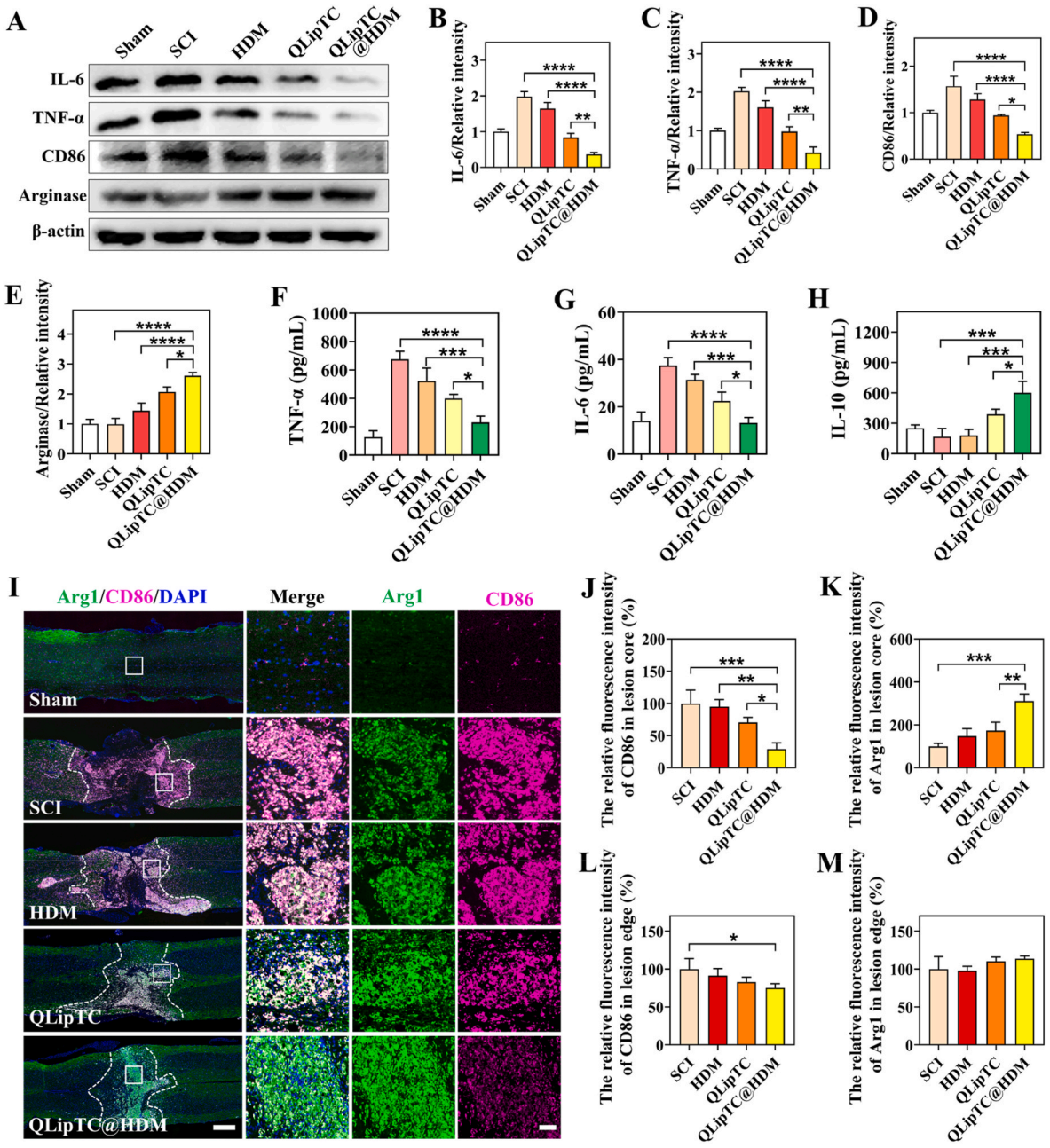

Fig. 5. QLipTC@HDM promotes the transformation of microglia to the M2 phenotype and inhibits the inflammatory response in mice following SCI. (A) Western blot analysis of IL-6, TNF-α, CD86, and Arginase protein expressions in spinal cord tissues 5 days post-SCI. (B–E) Quantitative analysis of IL-6, TNF-α, CD86, and Arginase protein levels. (F–H) ELISA analysis of the concentrations of IL-6, TNF-α, and IL-10 proteins in spinal cord tissues 5 days post-SCI. (I) Immunofluorescence images of CD86 (red), Arg1 (green), and DAPI (blue) in spinal cord tissues 5 days post-SCI. Scale bars are 500 μm (left) and 50 μm (right). Quantitative analysis of the mean fluorescence intensity of CD86 and Arg1 in the lesion core (J, K) and in the lesion edge (L, M). *for $p < 0.05$, ** for $p < 0.01$, *** for $p < 0.001$, **** for $p < 0.0001$.

the GelMA group exhibited gel migration and drug diffusion 24 h post-administration. This in situ delivery system is advantageous for drug storage at the target site, ensuring the maintenance of effective concentrations. Additionally, this enhances anti-inflammatory effects and facilitates the repair process. Our findings demonstrate that the application of QLipTC@HDM inhibits the conversion of glial cells to the M1 phenotype while promoting their transition to the M2 phenotype. Furthermore, this system facilitates the restoration of the BSCB, mitigates glial scarring, and enhances motor function recovery in mice with SCI. The therapeutic efficacy of QLipTC@HDM in the treatment of SCI exhibits a significant advantage, positioning it as a promising candidate for future SCI therapeutic interventions.

Although the application of QLipTC@HDM in the treatment of spinal cord injury (SCI) shows promise, it is accompanied by certain limitations. Notably, in clinical practice, there exists considerable individual variability among SCI patients, encompassing differences in injury severity, comorbid conditions, and genetic background. Furthermore, the uncontrolled release of drugs from QLipTC@HDM may adversely impact its therapeutic efficacy and safety profile. In the future, the development of smart materials with concealed, controllable, and responsive release properties—sensitive to stimuli such as pH, enzymes, and light, will facilitate the regulation of drug release, enable personalized therapy, and enhance medication safety management. Furthermore, the absence of direct comparative studies between QLipTC@HDM and other existing treatments for SCI, such as cell therapy and physical rehabilitation, constrains the evaluation of its relative efficacy and cost-

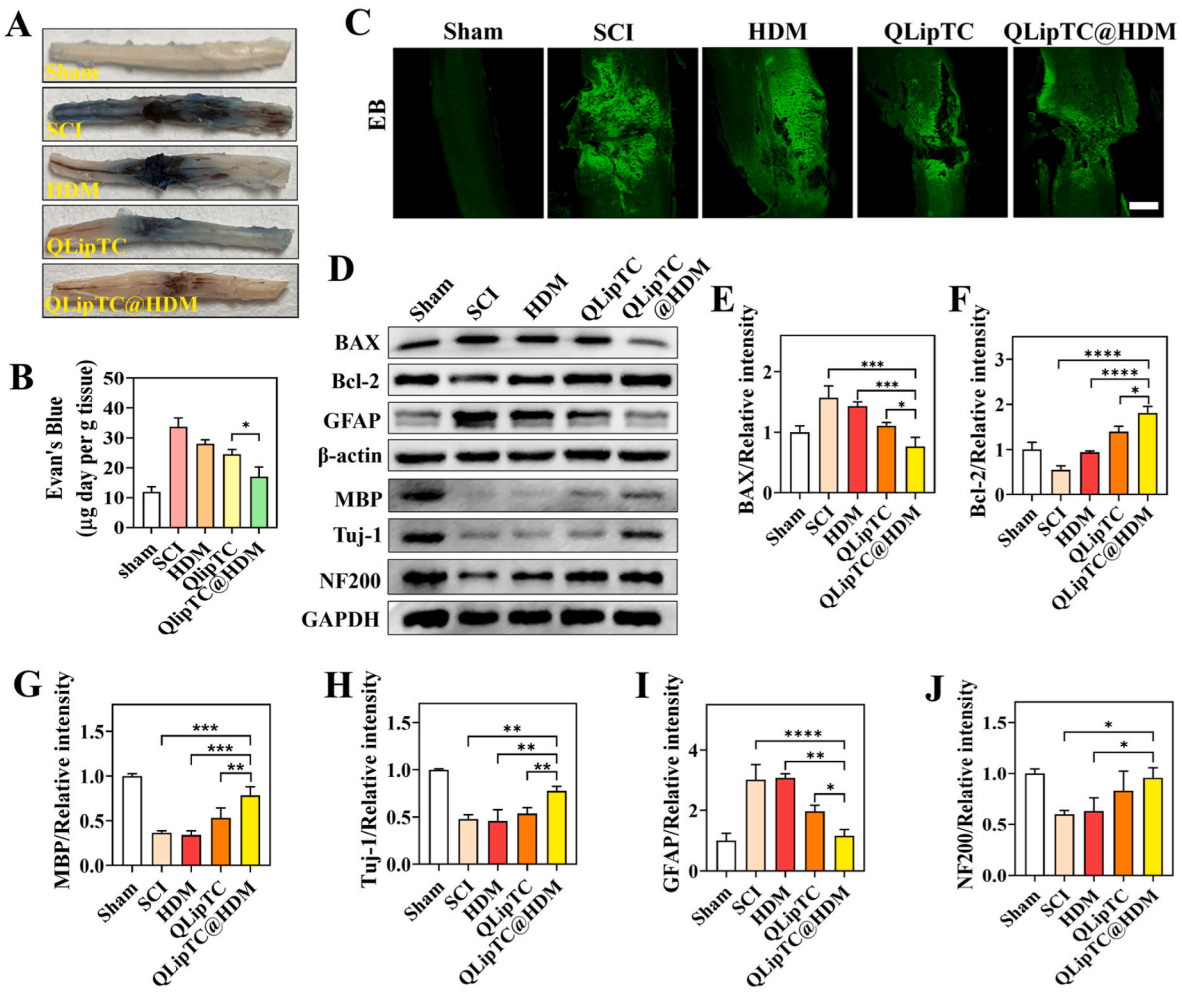

Fig. 6. QLipTC@HDM improves the microenvironment of spinal cord lesions, attenuates neuronal death, and suppresses glial scarring. (A) Representative images of the spinal cord tissue were acquired 1 h following the tail vein injection of Evans blue (EB) dye. (B) Quantitative analysis of EB content accumulated in spinal cord tissue. (C) Representative confocal images of spinal cord tissue were acquired 1 h following the tail vein injection of EB dye. The scale bar is 500 μm. (D) Western blot analysis of BAX, Bcl-2, MBP, Tuj-1, NF200, and GFAP protein expression in spinal cord tissues 28 days post-injury. (E–J) Quantitative analysis of BAX, Bcl-2, MBP, Tuj-1, NF200, and GFAP protein levels in each group *for $p < 0.05$, ** for $p < 0.01$, *** for $p < 0.001$, **** for $p < 0.0001$.

effectiveness. Additionally, existing studies predominantly concentrate on preclinical models, often overlooking the complexity and chronicity inherent in human physiology and the progression of SCI. Future research should aim to overcome these limitations by lengthening the observation period and undertaking clinical trials to assess the long-term durability of functional recovery and the safety and efficacy of QLipTC@HDM in human subjects.

In summary, this study highlights the potential of QLipTC@HDM as a disease-specific drug delivery system for SCI. Its ability to enhance drug solubility, reduce side effects, traverse the BSCB, target the lesion site, and promote a favorable microenvironment positions QLipTC@HDM as a promising therapeutic strategy. This advancement may address the intricate challenges associated with SCI, offering new avenues for research and clinical application and serving as a valuable reference for future investigations.

5. Conclusion

In this research, we developed a transmembrane-targeted lipid-based hydrogel drug delivery system (QLipTC@HDM) to enhance the therapeutic efficacy of Que in modulating neuroinflammation and improving spinal cord regeneration. The QLipTC@HDM system provides an innovative drug delivery platform for treating SCI by integrating liposomes (QLipTC) into dual network viscous hydrogels (HDM). Encapsulating Que within LipTC enhances its aqueous solubility and bioavailability, while simultaneously mitigating potential toxicities, offering a substantial benefit for its clinical applications. The development of dual-targeting liposomes (LipTC) improves the precision of drug delivery to the site of injury, facilitates the penetration of Que across the BSCB, and substantially enhances bioavailability. In addition, the use of HDM hydrogel significantly prolonged the retention time of QLipTC at the local injury site through in-situ delivery, which is of great significance for improving drug efficacy and reducing the frequency of drug administration. When applied to SCI, the QLipTC@HDM system has exhibited efficacy in promoting M2 polarization of microglia, enhancing the secretion of anti-inflammatory mediators, improving the integrity of the BSCB, facilitating axonal growth, reducing glial scar, and enhancing motor function in hind limbs following SCI. Considering the favorable outcomes observed with the QLipTC@HDM system in preclinical animal studies, this approach holds great potential as a therapeutic strategy for the clinical management of SCI, showing broad prospects for clinical application.

CRediT authorship contribution statement

Penghui Wang: Writing – original draft, Visualization, Resources, Investigation, Formal analysis. **Zaifeng Chen:** Writing – review & editing. **Ping Li:** Resources, Investigation. **Abdullah Al Mamun:**

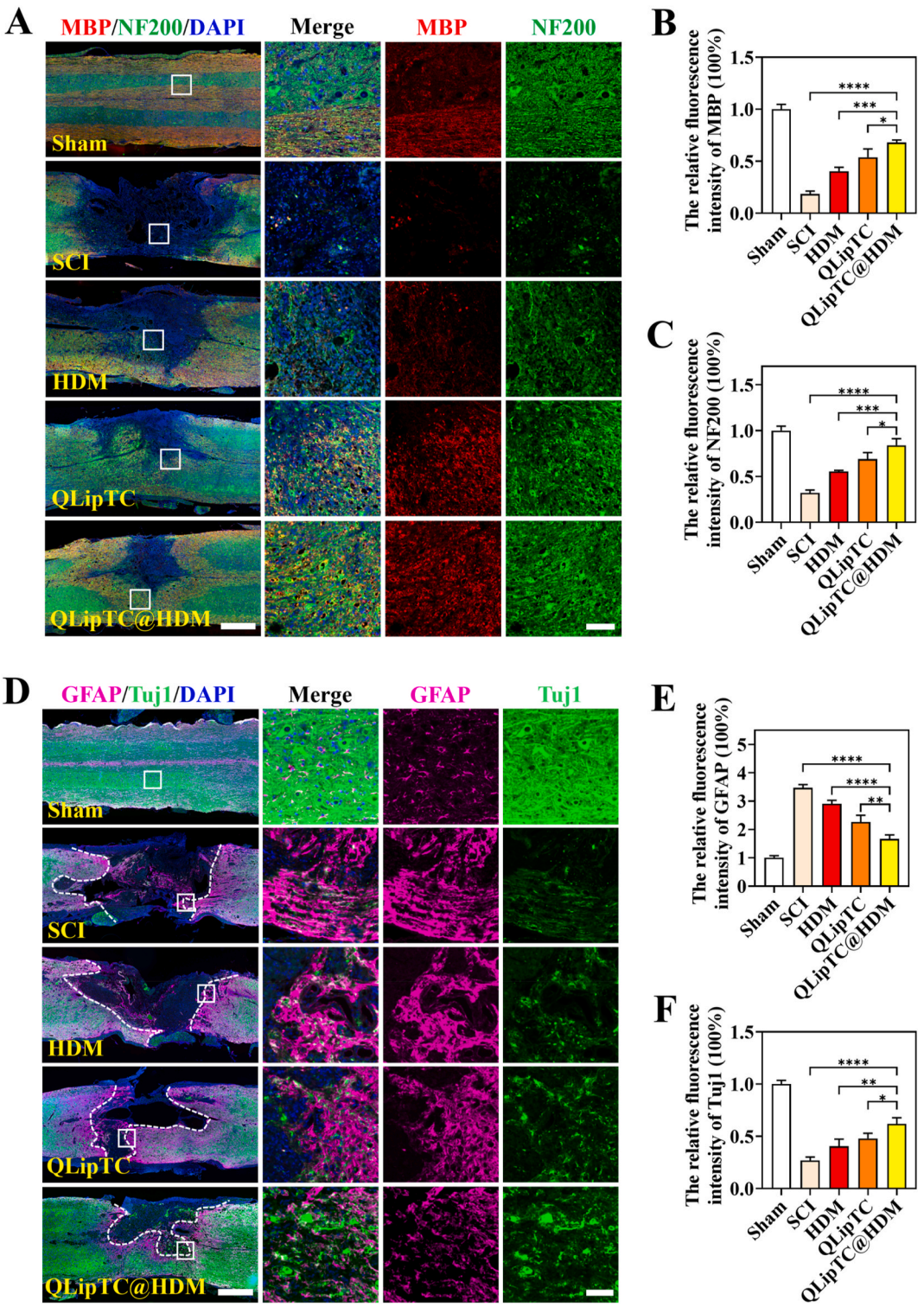

Fig. 7. QLipTC@HDM ameliorates damaged nerves and attenuates glial scarring. (A) Immunofluorescence images of MBP (red), NF200 (green), and DAPI (blue) in spinal cord tissues 28 days post-SCI. Scale bars are 500 μm (left) and 50 μm (right). (B, C) Quantitative analysis of the average fluorescence intensity of MBP and NF200. (D) Immunofluorescence images of GFAP (red), Tuj-1 (green), and DAPI (blue) in spinal cord tissues 28 days post-SCI. Scale bars are 500 μm (left) and 50 μm (right). (E, F) Quantitative analysis of the average fluorescence intensity of GFAP and Tuj-1. *for $p < 0.05$, ** for $p < 0.01$, *** for $p < 0.001$, **** for $p < 0.0001$.

Writing – review & editing. **Shaoxia Ning:** Resources, Investigation. **Jinjing Zhang:** Resources, Investigation, Funding acquisition. **Chonghui Tang:** Resources, Investigation. **Tianmiao Sun:** Resources, Investigation. **Jian Xiao:** Writing – review & editing. **Xiaojie Wei:** Supervision, Funding acquisition, Conceptualization. **Fenzan Wu:** Writing – review & editing, Visualization, Investigation.

Availability of data and materials

The datasets and material generated during and/or analyzed during the current study are available from the corresponding author upon reasonable request.

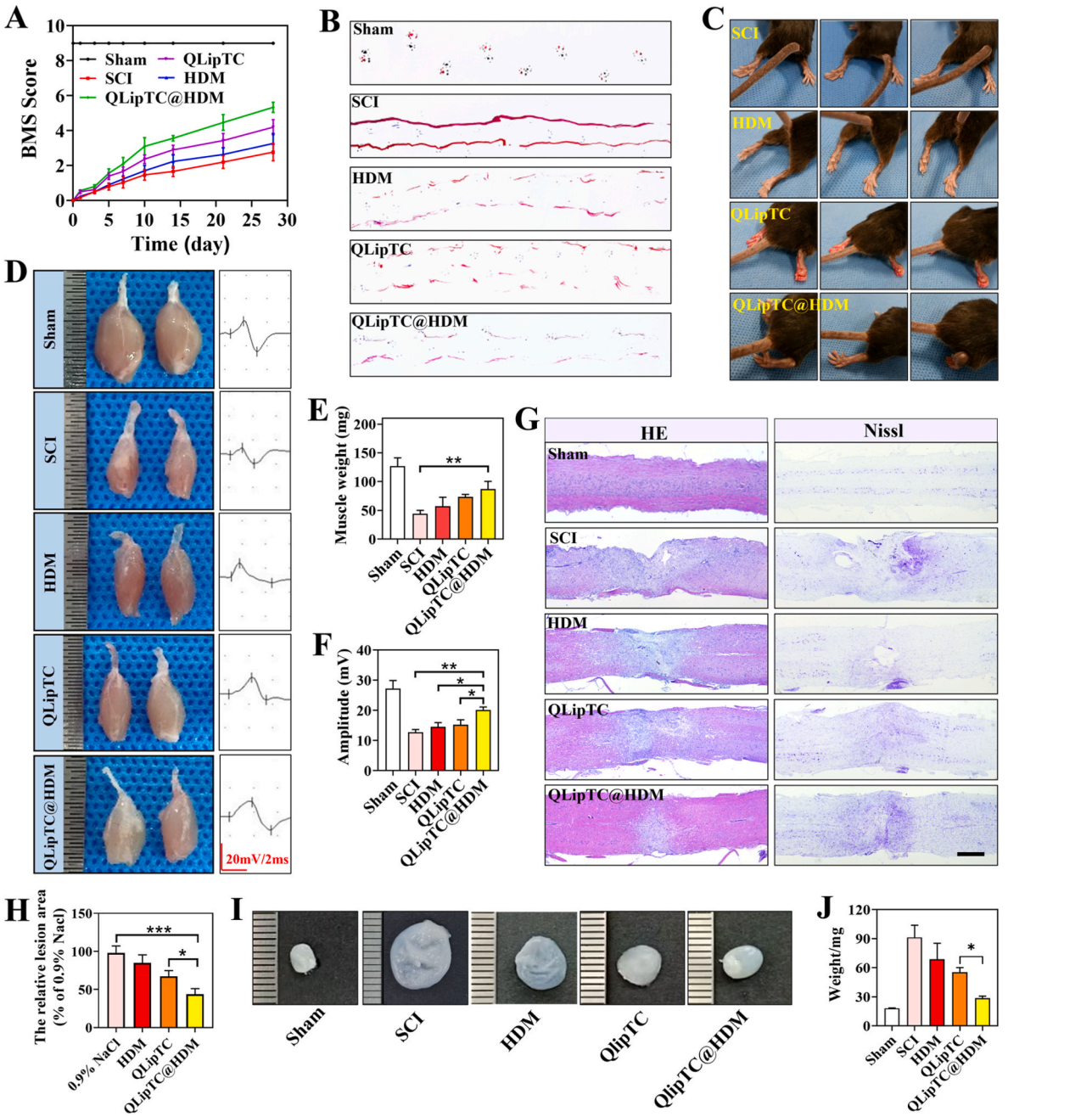

Fig. 8. QLipTC@HDM enhances motor function recovery and improves the morphology of injured tissues 28 days post-SCI. (A) BMS scores of mice in various groups. (B) Representative footprint images of mice from different groups. (C) Representative images of hindlimb movement in mice from different groups. (D) Representative images of the gastrocnemius muscle and MEPs in the hind limbs of mice from different groups. (E) Quantitative analysis of muscle weight. (F) Quantitative analysis of MEPs amplitude. (G) HE and Nissl staining images of spinal cord tissue 28 days post-SCI. The scale bar is 500 μm. (H) Quantitative analysis of cavity area according to HE staining. (I) Representative images of bladder tissue 28 days post-SCI. (J) Quantitative analysis of the weight of bladder tissue. *Represents $p < 0.05$, ** for $p < 0.01$, *** for $p < 0.001$.

Consent for publication

All contributing authors agree to the publication of this article.

Funding

This work was supported by the Basic Public Welfare Research Project of Zhejiang Province [grant number LYY21H300003], Medical and Health Technology Project of Zhejiang Province [grant number 2025KY1494], Natural Science Foundation of Ningbo [grant number 2024J470], Leading Medical & Health Discipline Project of Ningbo [grant number 2022-X21], Key Disciplines of Cixi City [grant number 2023-ZD03], Science and Technology Plan Project of Cixi City [grant number CN2023012, CN2023006].

Declaration of competing interest

The authors declare that they have no known competing financial interests or personal relationships that could have appeared to influence the work reported in this paper.

Appendix A. Supplementary data

Supplementary data to this article can be found online at https://doi.org/10.1016/j.mtbio.2025.101518.

Data availability

Data will be made available on request.

References

[1] C. Kathe, M.A. Skinnider, T.H. Hutson, N. Regazzi, M. Gautier, R. Demesmaeker, S. Komi, S. Ceto, N.D. James, N. Cho, L. Baud, K. Galan, K.J.E. Matson, A. Rowald, K. Kim, R. Wang, K. Minassian, J.O. Prior, L. Asboth, Q. Barraud, S.P. Lacour, A. J. Levine, F. Wagner, J. Bloch, J.W. Squair, G. Courtine, The neurons that restore walking after paralysis, Nature 611 (7936) (2022) 540–547, https://doi.org/10.1038/s41586-022-05385-7.

[2] C.M. Zipser, J.J. Cragg, J.D. Guest, M.G. Fehlings, C.R. Jutzeler, A.J. Anderson, A. Curt, Cell-based and stem-cell-based treatments for spinal cord injury: evidence from clinical trials, Lancet Neurol. 21 (7) (2022) 659–670, https://doi.org/10.1016/s1474-4422(21)00464-6.

[3] T. Tian, S. Zhang, M. Yang, Recent progress and challenges in the treatment of spinal cord injury, Protein Cell 14 (9) (2023) 635–652, https://doi.org/10.1093/procel/pwad003.

[4] C.M. Walsh, K. Gull, D. Dooley, Motor rehabilitation as a therapeutic tool for spinal cord injury: new perspectives in immunomodulation, Cytokine Growth Factor Rev. 69 (2023) 80–89, https://doi.org/10.1016/j.cytogfr.2022.08.005.

[5] Y. Li, Z. Lei, R.M. Ritzel, J. He, H. Li, H.M.C. Choi, M.M. Lipinski, J. Wu, Impairment of autophagy after spinal cord injury potentiates neuroinflammation and motor function deficit in mice, Theranostics 12 (12) (2022) 5364–5388, https://doi.org/10.7150/thno.72713.

[6] X. Hu, W. Xu, Y. Ren, Z. Wang, X. He, R. Huang, B. Ma, J. Zhao, R. Zhu, L. Cheng, Spinal cord injury: molecular mechanisms and therapeutic interventions, Signal Transduct Target Ther 8 (1) (2023) 245, https://doi.org/10.1038/s41392-023-01477-6.

[7] X. Freyermuth-Trujillo, J.J. Segura-Uribe, H. Salgado-Ceballos, C.E. Orozco-Barrios, A. Coyoy-Salgado, Inflammation: a target for treatment in spinal cord injury, Cells 11 (17) (2022) 2692, https://doi.org/10.3390/cells11172692.

[8] A.B. da Silva, P.L. Cerqueira Coelho, M. das Neves Oliveira, J.L. Oliveira, J. A. Oliveira Amparo, K.C. da Silva, J.R.P. Soares, B.P.S. Pitanga, C. Dos Santos Souza, G.P. de Faria Lopes, V.D.A. da Silva, M. de Fátima Dias Costa, M.P. Junier, H. Chneiweiss, V. Moura-Neto, S.L. Costa, The flavonoid rutin and its aglycone quercetin modulate the microglia inflammatory profile improving antiglioma activity, Brain Behav. Immun. 85 (2020) 170–185, https://doi.org/10.1016/j.bbi.2019.05.003.

[9] H. Fan, H.B. Tang, L.Q. Shan, S.C. Liu, D.G. Huang, X. Chen, Z. Chen, M. Yang, X. H. Yin, H. Yang, D.J. Hao, Quercetin prevents necroptosis of oligodendrocytes by inhibiting macrophages/microglia polarization to M1 phenotype after spinal cord injury in rats, J. Neuroinflammation 16 (1) (2019) 206, https://doi.org/10.1186/s12974-019-1613-2.

[10] X. Han, T. Xu, Q. Fang, H. Zhang, L. Yue, G. Hu, L. Sun, Quercetin hinders microglial activation to alleviate neurotoxicity via the interplay between NLRP3 inflammasome and mitophagy, Redox Biol. 44 (2021) 102010, https://doi.org/10.1016/j.redox.2021.102010.

[11] L. Li, W. Jiang, B. Yu, H. Liang, S. Mao, X. Hu, Y. Feng, J. Xu, L. Chu, Quercetin improves cerebral ischemia/reperfusion injury by promoting microglia/macrophages M2 polarization via regulating PI3K/Akt/NF-κB signaling pathway, Biomed. Pharmacother. 168 (2023) 115653, https://doi.org/10.1016/j.biopha.2023.115653.

[12] D. Sun, Y. Zou, L. Song, S. Han, H. Yang, D. Chu, Y. Dai, J. Ma, C.M. O'Driscoll, Z. Yu, J. Guo, A cyclodextrin-based nanoformulation achieves co-delivery of ginsenoside Rg3 and quercetin for chemo-immunotherapy in colorectal cancer, Acta Pharm. Sin. B 12 (1) (2022) 378–393, https://doi.org/10.1016/j.apsb.2021.06.005.

[13] L. Guo, Z. Huang, L. Huang, J. Liang, P. Wang, L. Zhao, Y. Shi, Surface-modified engineered exosomes attenuated cerebral ischemia/reperfusion injury by targeting the delivery of quercetin towards impaired neurons, J. Nanobiotechnol. 19 (1) (2021) 141, https://doi.org/10.1186/s12951-021-00879-4.

[14] J. Cen, R. Zhang, T. Zhao, X. Zhang, C. Zhang, J. Cui, K. Zhao, S. Duan, Y. Guo, A water-soluble quercetin conjugate with triple targeting exerts neuron-protective effect on cerebral ischemia by mitophagy activation, Adv. Healthc. Mater. 11 (22) (2022) e2200817, https://doi.org/10.1002/adhm.202200817.

[15] E.M. Tomou, P. Papakyriakopoulou, E.M. Saitani, G. Valsami, N. Pippa, H. Skaltsa, Recent advances in nanoformulations for quercetin delivery, Pharmaceutics 15 (6) (2023) 1656, https://doi.org/10.3390/pharmaceutics15061656.

[16] J.J. Ma, X.N. Huang, S.W. Yin, Y.G. Yu, X.Q. Yang, Bioavailability of quercetin in zein-based colloidal particles-stabilized Pickering emulsions investigated by the in vitro digestion coupled with Caco-2 cell monolayer model, Food Chem. 360 (2021) 130152, https://doi.org/10.1016/j.foodchem.2021.130152.

[17] X.R. Xu, H.T. Yu, Y. Yang, L. Hang, X.W. Yang, S.H. Ding, Quercetin phospholipid complex significantly protects against oxidative injury in ARPE-19 cells associated with activation of Nrf2 pathway, Eur. J. Pharmacol. 770 (2016) 1–8, https://doi.org/10.1016/j.ejphar.2015.11.050.

[18] T.H. Tran, Y. Guo, D. Song, R.S. Bruno, X. Lu, Quercetin-containing self-nanoemulsifying drug delivery system for improving oral bioavailability, J. Pharm. Sci. 103 (3) (2014) 840–852, https://doi.org/10.1002/jps.23858.

[19] Y.J. Guo, F. Yang, L. Zhang, J. Pi, J.Y. Cai, P.H. Yang, Facile synthesis of multifunctional germanium nanoparticles as a carrier of quercetin to achieve enhanced biological activity, Chem. Asian J. 9 (8) (2014) 2272–2280, https://doi.org/10.1002/asia.201402227.

[20] S. Shah, V. Dhawan, R. Holm, M.S. Nagarsenker, Y. Perrie, Liposomes: advancements and innovation in the manufacturing process, Adv. Drug Deliv. Rev. 154–155 (2020) 102–122, https://doi.org/10.1016/j.addr.2020.07.002.

[21] M. Dymek, E. Sikora, Liposomes as biocompatible and smart delivery systems - the current state, Adv. Colloid Interface Sci. 309 (2022) 102757, https://doi.org/10.1016/j.cis.2022.102757.

[22] T. Kurano, T. Kanazawa, A. Ooba, Y. Masuyama, N. Maruhana, M. Yamada, S. Iioka, H. Ibaraki, Y. Kosuge, H. Kondo, T. Suzuki, Nose-to-brain/spinal cord delivery kinetics of liposomes with different surface properties, J. Contr. Release 344 (2022) 225–234, https://doi.org/10.1016/j.jconrel.2022.03.017.

[23] K. Zhu, Y. Xu, R. Zhong, W. Li, H. Wang, Y.S. Wong, S. Venkatraman, J. Liu, Y. Cao, Hybrid liposome-erythrocyte drug delivery system for tumor therapy with enhanced targeting and blood circulation, Regen. Biomater. 10 (2023) rbad045, https://doi.org/10.1093/rb/rbad045.

[24] F. Wu, P. Wang, X. Wei, Y. Yang, A. Al Mamun, X. Zhang, Y. Zhu, T. Mo, H. Zhang, C. Jiang, J. Hu, J. Xiao, Barrier-penetrating liposome targeted delivery of basic fibroblast growth factor for spinal cord injury repair, Mater. Today Bio 18 (2023) 100546, https://doi.org/10.1016/j.mtbio.2023.100546.

[25] J. Chen, J. Chen, P. Yu, C. Yang, C. Xia, J. Deng, M. Yu, Z. Xiang, L. Gan, B. Zhu, Y. Wu, X. Yang, A novel quercetin encapsulated glucose modified liposome and its brain-target antioxidative neuroprotection effects, Molecules 29 (3) (2024) 607, https://doi.org/10.3390/molecules29030607.

[26] C. Yang, T. Xu, Y. Lu, J. Liu, C. Chen, H. Wang, X. Chen, Quercetin-loaded human umbilical cord mesenchymal stem cell-derived sEVs for spinal cord injury recovery, Neuroscience 552 (2024) 14–28, https://doi.org/10.1016/j.neuroscience.2024.05.028.

[27] F. Lv, J. Wang, H. Chen, L. Sui, L. Feng, Z. Liu, Y. Liu, G. Wei, W. Lu, Enhanced mucosal penetration and efficient inhibition efficacy against cervical cancer of PEGylated docetaxel nanocrystals by TAT modification, J. Contr. Release 336 (2021) 572–582, https://doi.org/10.1016/j.jconrel.2021.07.008.

[28] S. Clement, A.G. Anwer, L. Pires, J. Campbell, B.C. Wilson, E.M. Goldys, Radiodynamic therapy using TAT peptide-targeted verteporfin-encapsulated PLGA nanoparticles, Int. J. Mol. Sci. 22 (12) (2021) 6425, https://doi.org/10.3390/ijms22126425.

[29] L. Zhao, L. Ling, J. Lu, F. Jiang, J. Sun, Z. Zhang, Y. Huang, X. Liu, Y. Zhu, X. Fu, S. Peng, W. Yuan, R. Zhao, Z. Zhang, Reactive oxygen species-responsive mitochondria-targeted liposomal quercetin attenuates retinal ischemia-reperfusion injury via regulating SIRT1/FOXO3A and p38 MAPK signaling pathways, Bioeng. Transl. Med. 8 (3) (2023) e10460, https://doi.org/10.1002/btm2.10460.

[30] T. Li, P. Jing, L. Yang, Y. Wan, X. Du, J. Wei, M. Zhou, Z. Liu, Y. Lin, Z. Zhong, CAQK modification enhances the targeted accumulation of metformin-loaded nanoparticles in rats with spinal cord injury, Nanomedicine 41 (2022) 102526, https://doi.org/10.1016/j.nano.2022.102526.

[31] Y. Rong, Z. Wang, P. Tang, J. Wang, C. Ji, J. Chang, Y. Zhu, W. Ye, J. Bai, W. Liu, G. Yin, L. Yu, X. Zhou, W. Cai, Engineered extracellular vesicles for delivery of siRNA promoting targeted repair of traumatic spinal cord injury, Bioact. Mater. 23 (2023) 328–342, https://doi.org/10.1016/j.bioactmat.2022.11.011.

[32] J. Wang, D. Li, C. Liang, C. Wang, X. Zhou, L. Ying, Y. Tao, H. Xu, J. Shu, X. Huang, Z. Gong, K. Xia, F. Li, Q. Chen, J. Tang, Y. Shen, Scar tissue-targeting polymer micelle for spinal cord injury treatment, Small 16 (8) (2020) e1906415, https://doi.org/10.1002/smll.201906415.

[33] S. Zhang, Q. Li, S. Zhang, Neural regeneration ability of Polypyrrole-Collagen-Quercetin composite in the spinal cord injury, Regen. Ther. 24 (2023) 85–93, https://doi.org/10.1016/j.reth.2023.05.010.

[34] D.K. Patel, K. Ganguly, J. Hexiu, S.D. Dutta, T.V. Patil, K.T. Lim, Functionalized chitosan/spherical nanocellulose-based hydrogel with superior antibacterial efficiency for wound healing, Carbohydr. Polym. 284 (2022) 119202, https://doi.org/10.1016/j.carbpol.2022.119202.

[35] R.L. Alexa, H. Iovu, B. Trica, C. Zaharia, A. Serafim, E. Alexandrescu, I.C. Radu, G. Vlasceanu, S. Preda, C.M. Ninciuleanu, R. Ianchis, Assessment of naturally sourced mineral clays for the 3D printing of biopolymer-based nanocomposite inks, Nanomaterials 11 (3) (2021) 703, https://doi.org/10.3390/nano11030703.

[36] D. Xu, L.N. Gao, X.J. Song, Q.W. Dong, Y.B. Chen, Y.L. Cui, Q. Wang, Enhanced antidepressant effects of BDNF-quercetin alginate nanogels for depression therapy, J. Nanobiotechnol. 21 (1) (2023) 379, https://doi.org/10.1186/s12951-023-02150-4.

[37] D. Sonawane, V. Pokharkar, Quercetin-loaded nanostructured lipid carrier in situ gel for brain targeting through intranasal route: formulation, in vivo pharmacokinetic and pharmacodynamic studies, AAPS PharmSciTech 25 (2) (2024) 30, https://doi.org/10.1208/s12249-024-02736-7.

[38] J. Chen, D. Wang, L.H. Wang, W. Liu, A. Chiu, K. Shariati, Q. Liu, X. Wang, Z. Zhong, J. Webb, R.E. Schwartz, N. Bouklas, M. Ma, An adhesive hydrogel with "Load-Sharing" effect as tissue bandages for drug and cell delivery, Adv. Mater. 32 (43) (2020) e2001628, https://doi.org/10.1002/adma.202001628.

[39] J. Chen, J.S. Caserto, I. Ang, K. Shariati, J. Webb, B. Wang, X. Wang, N. Bouklas, M. Ma, An adhesive and resilient hydrogel for the sealing and treatment of gastric perforation, Bioact. Mater. 14 (2022) 52–60, https://doi.org/10.1016/j.bioactmat.2021.11.038.

[40] Y. Ode, A.R. Pradipta, P. Ahmadi, A. Ishiwata, A. Nakamura, Y. Egawa, Y. Kusakari, K. Muguruma, Y. Wang, X. Yin, N. Sato, H. Haba, K. Tanaka, Therapeutic efficacy of (211)At-radiolabeled 2,6-diisopropylphenyl azide in mouse models of human lung cancer, Chem. Sci. 14 (30) (2023) 8054–8060, https://doi.org/10.1039/d3sc02513f.

[41] K.D. Patel, S.A. Mohid, A. Dutta, S. Arichthota, A. Bhunia, D. Haldar, V. Sarojini, Synthesis and antibacterial study of cell-penetrating peptide conjugated trifluoroacetyl and thioacetyl lysine modified peptides, Eur. J. Med. Chem. 219 (2021) 113447, https://doi.org/10.1016/j.ejmech.2021.113447.

[42] X. Chen, B. Wang, Y. Zhou, X. Wu, A. Du, A. Al Mamun, Y. Xu, S. Wang, C. Jiang, L. Xie, K. Zhou, S. Hu, J. Xiao, Poly (betulinic acid) nanoparticles loaded with bFGF improve functional recovery after spinal cord injury, Adv. Healthc. Mater. 13 (12) (2024) e2303462, https://doi.org/10.1002/adhm.202303462.

[43] N. Suganthy, K.P. Devi, S.F. Nabavi, N. Braidy, S.M. Nabavi, Bioactive effects of quercetin in the central nervous system: focusing on the mechanisms of actions, Biomed. Pharmacother. 84 (2016) 892–908, https://doi.org/10.1016/j.biopha.2016.10.011.

[44] M.C. Chiang, T.Y. Tsai, C.J. Wang, The potential benefits of quercetin for brain Health: a review of anti-inflammatory and neuroprotective mechanisms, Int. J. Mol. Sci. 24 (7) (2023) 6328, https://doi.org/10.3390/ijms24076328.

[45] S.H. Liu, Y. Han, X.J. Liu, R.L. Wang, B. Sun, A. Nakabayashi, J.L. Chai, D.J. Li, Improving the solubilization, stability, dialysis performance and antioxidant properties of quercetin in surfactant-free microemulsion, J. Mol. Liq. 409 (2024) 125531, https://doi.org/10.1016/j.molliq.2024.125531.

[46] X. Chen, D.J. McClements, Y. Zhu, Y. Chen, L. Zou, W. Liu, C. Cheng, D. Fu, C. Liu, Enhancement of the solubility, stability and bioaccessibility of quercetin using protein-based excipient emulsions, Food Res. Int. 114 (2018) 30–37, https://doi.org/10.1016/j.foodres.2018.07.062.

[47] A.I. Oliveira, C. Pinho, B. Sarmento, A.C.P. Dias, Quercetin-biapigenin nanoparticles are effective to penetrate the blood-brain barrier, Drug Deliv. Transl. Res. 12 (1) (2022) 267–281, https://doi.org/10.1007/s13346-021-00917-6.